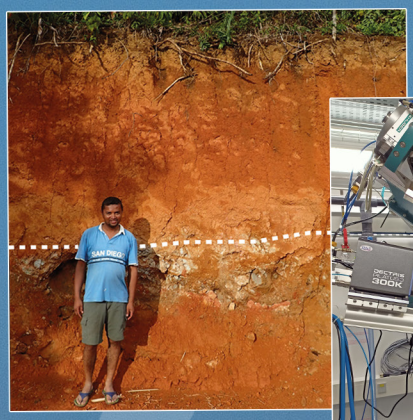

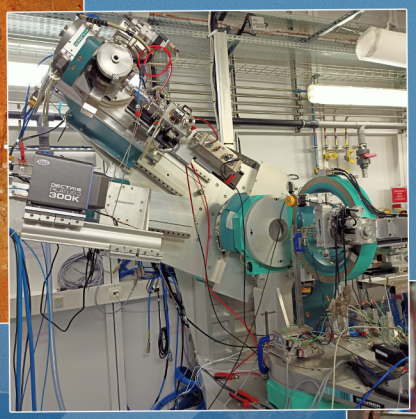

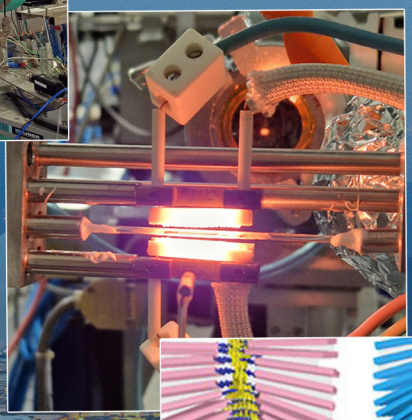

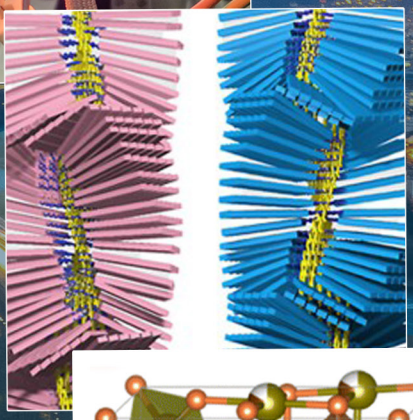

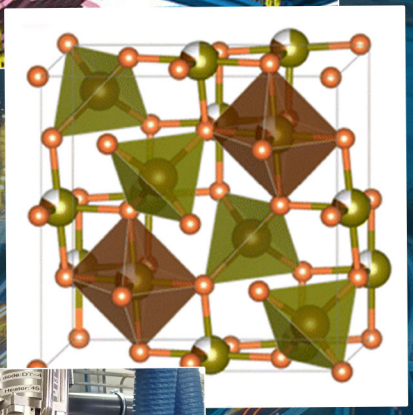

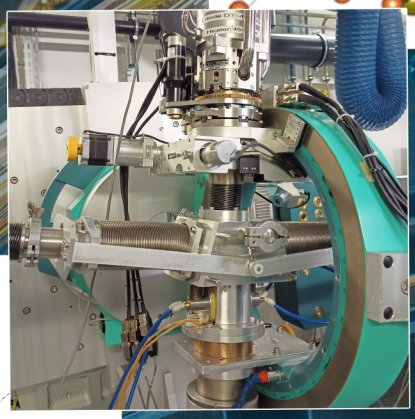

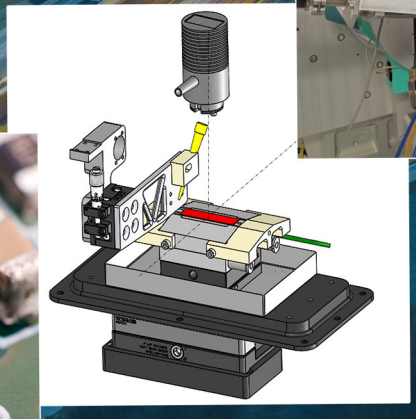

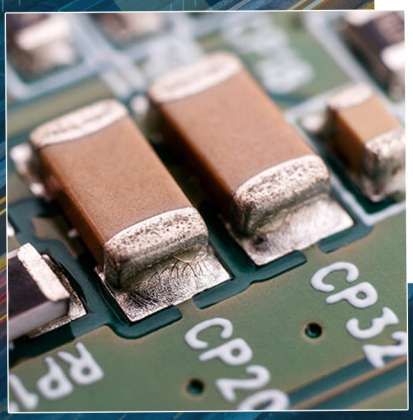

NEWSLETTER 2025

XMaS

The UK Materials Science Beamline

CONTENTS

ON THE COVER:
The science portfolio on XMaS embraces a broad range of scientific disciplines some of them being presented in the present Newsletter edition.
Aerial view of ESRF. Credit ESRF/vuedici.org

Advancing Science at XMaS

It has been a busy and productive year at the XMaS beamline with a number of technical developments running alongside a full user programme of experiments. During 2025, we optimised some of our metrologies to enhance operational efficiency. New multi sample stages were introduced, including a multi capillary holder, a transmission rack accommodating up to thirty pellets and a grazing incidence stage capable of hosting six samples. These upgrades, together with streamlined alignment routines, now support faster and more reliable operations and were used for the newly established BAG (Block Allocation Group) access mode. The BAG focuses on high throughput of samples within energy materials and catalysis, and is co-hosted with B18 at Diamond Light Source, allowing samples to be allocated to the most scientifically appropriate beamline (see more details in the *Facility Updates* section in page 3). This approach is supported using an identical sample holder at both beamlines, which removes barriers to sample transfer and ensures a smooth and seamless user experience.

There remains a growing user demand for complex *operando* and *in-situ* experiments, particularly those requiring gas-based sample environments which create complex, dynamic conditions and enable chemical reactions to be monitored in real time. The gas handling system, developed in collaboration with the UK Catalysis Hub, is in its final stage of being installed on the beamline and should be available to users after approval from ESRF Safety Group-hopefully by Spring 2026. To ensure full compliance with safety requirements, an extraction system was integrated directly into the air handling infrastructure. The system removes any minor leaks and prevents the accumulation of hazardous gases in the experimental hutch.

XMaS was originally conceived as a magnetic scattering beamline and was equipped with a comprehensive suite of magnets that could be mounted directly onto the diffractometer. Delivery of a new 1 T magnet is anticipated at the end of 2026. We are also awaiting the delivery of the new low temperature JT cryostat that fits inside the 4 T magnet; this will enable us to regain our sub 10 K & 4 T field environment capability and is expected in the Summer.

XMaS has a long-standing track record of enabling measurements under applied strain. Building on this expertise, and in collaboration with colleagues at the APS we have designed and delivered a bespoke configuration in which a RazorBill FC1X0 strain cell was mounted onto one of our cryostats. The new sample environment allows offline and X-ray based measurements as a function of temperature and applied strain. This demonstrator experiment (see article page 5) generated considerable interest within our user community. In response, we have now procured our own RazorBill cell and capacitance meter and are integrating both into the XMaS control system.

In 2025, XMaS began its transition to BLISS, the ESRF's de facto control system for all beamlines. Several user experiments have already been successfully conducted under BLISS across a range of techniques including diffraction, SAXS, WAXS and reflectivity. In addition, and working closely with ESRF developers, new device servers will be deployed for the energy dispersive detectors and potentiostats. This programme will ensure that XMaS is fully aligned with ESRF control system standards by the end of 2026. Many thanks to the users who helped us running the first test experiments in real conditions!

It was a relatively quiet year in terms of personnel changes at XMaS. We did, however, say goodbye to Sophie Wawman, who was based at Warwick and provided administrative and user support. Thanks to Sophie for her contribution to the project and we wish her all the best for the future. Welcome to her replacement, Katherine Norman, who joined the team at the beginning of 2026.

In terms of outreach, the 11th edition of the *XMaS Scientist Experience* **[1]** was launched in December 2025 and we look forward to welcoming the winners to the ESRF in June. We also held the XMaS User Meeting in the Spine Building in Liverpool in January 2026 and this was attended by ~50 XMaS users and staff. The meeting showcased the broad range of material science that is conducted on the beamline. We look forward to another productive year of science in 2026!

Chris Lucas, Tom Hase, Yvonne Grunder and Malcolm Cooper

[1] www.xmas.ac.uk/impact/xmas_scientist_experienceb/

Materials BAG @XMaS

A Materials BAG (Block Allocation Group) is being implemented at XMaS/BM28 to support users exploiting spectroscopic studies. This new access route complements and runs alongside the existing Energy and Catalysis BAGs at B18@DLS.

Since the ESRF EBS upgrade, the operational energy of XMaS ranges from 2.035 to 47 keV, exploiting both transmission and fluorescence XAS modes. The XMaS Materials BAG is split into three categories:

- High Energy BAG (17 - 47 keV),
- Middle Energy BAG (5 - 17 keV),
- Low Energy BAG (E < 5 keV), the later implying a specific setup.

The BAG is coordinated by Dr. Maria Alfredsson from the University of Kent (**m.l.alfredssson@kent.ac.uk**). The experiment and data collection are run by the University of Kent and the XMaS staff.

More details about the XMaS BAG, including how to apply, are available on our website **[1]**. **Only** applications for **ex-situ samples** will be considered. The sample rack is identical to that used on B18. A video explaining how to prepare good pellets is also available. **The BAG application process is continuous.**

[1] www.xmas.ac.uk/applying_for_beamline_time/bag/

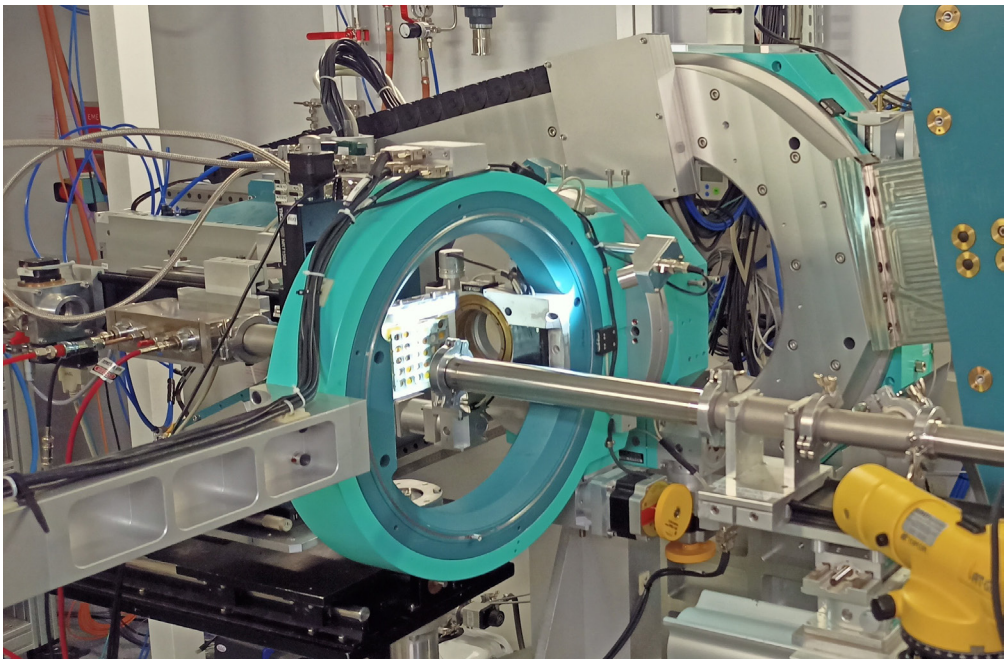

Fig. 1: XMaS Material BAG setup consisting of a 6 x 5 pellet rack mounted on a X-Z translation stage. Transmission mode showed here. Fluorescence mode also available and measured with either a 4-element Hitach Vortex SSD or a 7-element Mirion HPGe detector depending on the energy range. For the Low Energy BAG, a He/vacuum capatible 'ball' chamber incorporating a single element Ketek SSD is used instead.

Data handling & reduction

We are gradually migrating from SPEC to BLISS, the new ESRF control system. Custom macros to controll specific equipment (e.g. arbitrary waveform generator, phase-plate flipper, etc...) and others to allow diffraction and scattering studies with the PSIC geometry are being implemented within BLISS. On the other hand, (GI) SAXS/WAXS experiments are now carried out exclusively in BLISS and use a new data format. The data are stored in HDF5 files, following the NEXUS standard format **[1]** and can be handled by many programming languages and applications including Python, C, Fortran, pyMca, silx-view, DAWN, Igor-Pro and MATLAB etc.

We have developed a series of Python scripts and Jupyter notebooks built on the pyFAI python library **[2]** to transform the acquired images from the experimental geometry (2D images in pixel coordinates) into more suitable coordinate systems for further analysis (azimuthal angle vs. momentum transfer or scattering angle, perpendicular versus parallel momentum transfer...). Raw data can also be azimuthally integrated to yield 1D curves (intensity vs. momentum transfer or scattering angle). Currently, the data reduction process requires minimal intervention from the user and may be run in batch mode. In the near future, all processing steps will be performed automatically as data are acquired, using the EWOKS ESRF Workflow management system **[3]**.

The XMaS public software repository, which is being expanded over time, is accessible at **[4]**.

[1] https://www.nexusformat.org/
[2] https://pyfai.readthedocs.io/en/stable/
[3] https://ewoks.readthedocs.io/en/stable/
[4] https://gitlab.esrf.fr/xmas-bm28

Blade coater for GI-WAXS

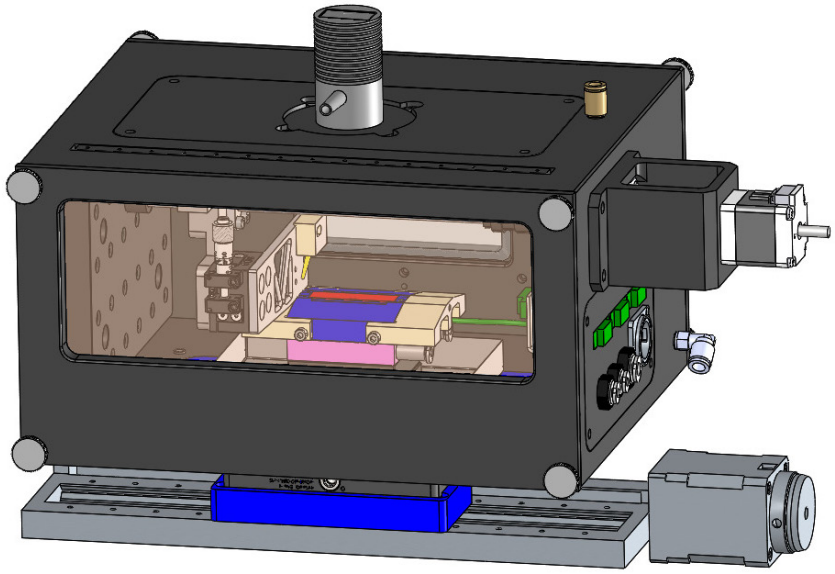

Fig. 2: 3D model of the blade coater designed for XMaS by the company 6TEC [1].

Solution-processed films such as polymers, small molecules, nanoparticles and perovskites are promising systems for a wide range of technologies, from paints and coatings to optoelectronic devices such as solar cells and light-emitting diodes. Their compatibility with large-area printing and coating techniques makes them attractive for scalable, low-cost manufacturing. However, many of the fundamental processes governing film formation and self-assembly — and the resulting film functionality — remain poorly understood.

To address this challenge, a new blade-coating chamber is currently being built at XMaS/BM28 to enable in-situ GI-WAXS/SAXS measurements during thin-film deposition (**Fig. 2** and **3**). In a typical experiment, a small volume of solution is deposited onto a substrate via a syringe pump and spread using a motorised blade, while the evolving film structure is monitored in real time during solvent evaporation. Optional sample heating during or after coating allows temperature-dependent studies, enabling users to directly link processing conditions to crystallisation, phase separation and nanoscale ordering.

A key feature of the chamber is an offset blade geometry (**Fig. 3**), which leaves the film accessible from above. This enables complementary *in-situ* or *operando* measurements, such as illumination during drying to study film stability under realistic operating conditions. The chamber has a highly modular architecture, allowing it to be adapted to the specific requirements of future experiments and emerging user needs.

The blade-coating chamber is expected to be available to users from September 2026, providing new opportunities for real-time studies of solution-processed materials at XMaS.

[1] www.6tec.fr

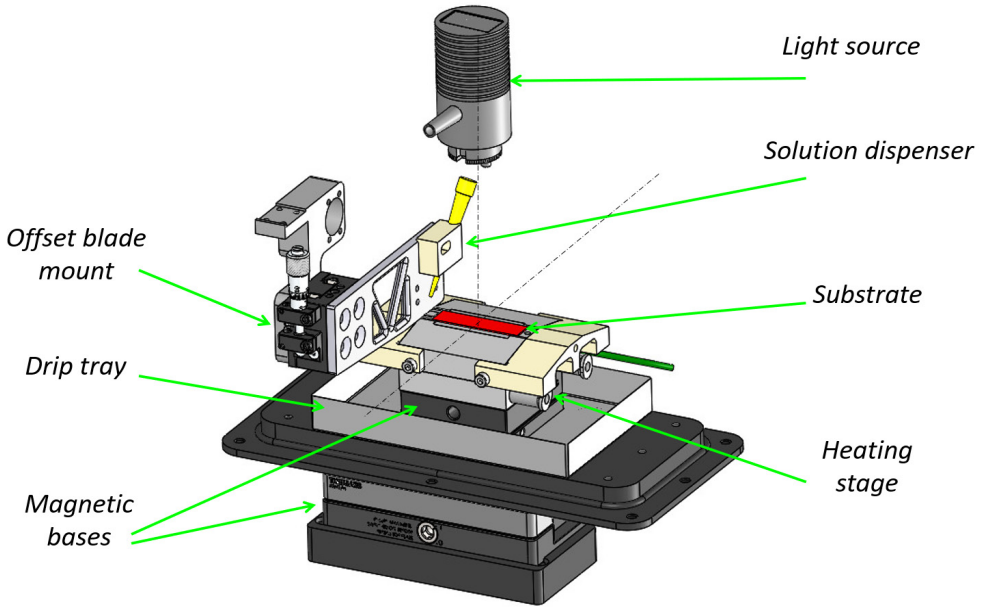

Fig. 3: Inside view of the actual blade coater allowing measurements between room temperature and 200°C.

Evidence for multicomponent superconductivity in Co-doped $BaFe_2As_2$

S. Ghosh, M.S. Ikeda, A.R. Chakraborty, T. Worasaran, F. Theuss, L.B. Peralta, P.M. Lozano, J.-W. Kim, P.J. Thompson, P.J. Ryan, L. Ye, A. Kapitulnik, S.A. Kivelson, B.J. Ramshaw, R.M. Fernandes, I.R. Fisher

The phase diagrams of most high-T_c superconductors (SC) are composed of multiple phases, which may cooperate or compete with the SC phase. In many iron-based SCs, for example, SC lies close to a nematic phase and the SC T_c is often seen to be maximised where nematic fluctuations are the strongest **[1]**. The interaction between nematic and SC phase is thus expected to provide crucial insights into the mechanism of SC in these materials.

We have studied the iron-based SC, Co-doped $BaFe_2As_2$ (see **Fig. 4**), utilising external strain to tune through its multiple phases. Using a Razorbill CS-100 strain cell, we perform a thermodynamic measurement, the AC elastocaloric effect (ECE), which is an extremely sensitive probe of phase transitions under strain. For greater than optimal doping (~6.2 %), we find a single phase transition from metallic to superconducting state, as expected. On the underdoped side but close to optimal doping, we find three transitions, one from tetragonal to orthorhombic (nematic transition) at T_S, the superconducting transition at T_c and a new phase transition inside the SC phase at T^*. To understand how this sequence of phase transitions affects the crystal structure of the material, we performed high-resolution X-ray diffraction (XRD) measurements at XMaS/BM28.

XRD measurements on a slightly underdoped (5.6 %) sample are shown in **Fig. 5**. The diffraction measurements were performed using a Pilatus3 300K detector with the sample in an ARS DE202 cryostat. Temperature dependence of θ - 2θ scans around the (2 2 6) reflection was measured. A clear splitting of the Bragg peak around T_S = 38 K indicates the tetragonal-to-orthorhombic transition. The increase in the splitting mimics the growth of nematicity and starts decreasing around T_c = 22 K, when superconductivity condenses and competes with nematicity **[2]**. However, no sharp feature is observed at $T^* \approx 19$ K, and the sample stays orthorhombic till the lowest temperatures (~14 K).

Ruling out any structural changes at T^*, we showed that the best candidate is time-reversal symmetry breaking at T^* **[3]** which requires a multicomponent SC state. Our findings show a crucial role of nematicity in determining optimal T_c as well as rendering the SC state fundamentally different in the underdoped regime. Further investigations are underway to understand the details of this novel multicomponent SC state.

[1] R. M. Fernandes *et al.*, Nature 601, 35 (2022).
[2] S. Nandi *et al.*, Phys. Rev. Lett. 104, 057006 (2010).
[3] S. Ghosh *et al.*, Proc. Natl. Acad. Sci. USA 122, e2424833122 (2025).

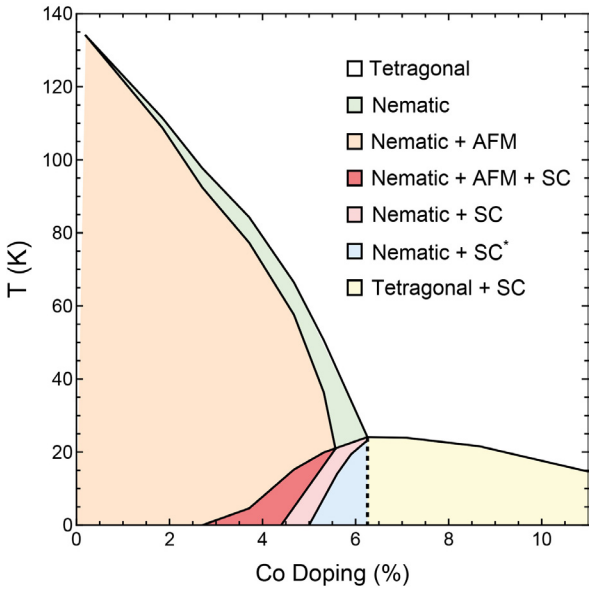

Fig. 4: Phase diagram of Co-doped $BaFe_2As_2$ based on existing and present data. SC* is the new phase that was discovered. AFM = Antiferromagnet.

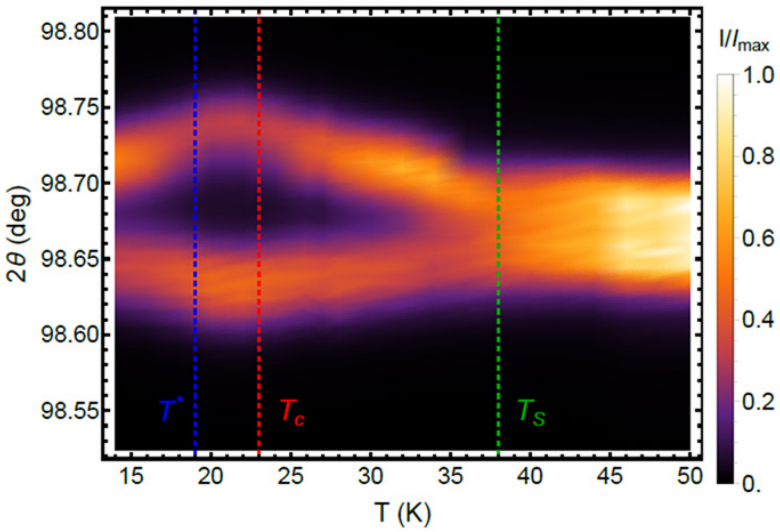

Fig. 5: Temperature evolution for the (2 2 6) Bragg peak for a 5.6 % sample on cooldown. The marked lines show expected transition temperatures, known from resistance and ECE measurements on similar doping sample. Incident X-ray energy of 6.977 keV was used.

For more information, contact:
S. Ghosh,
Department of Applied Physics,
Stanford University, USA.
sg2235@cornell.edu

Mapping magnetisation through compositionally graded rare-earth/transition-metal ferrimagnetic alloy thin films for spintronics

D. Rianto, B. Nicholson, A.W. Hodgkiss, A.J. Caruana, C.J. Kinane, L. Bouchenoire, P.P. Michałowski, T.P.A. Hase, D. Atkinson

Ferrimagnetic (FiM) materials have two opposing magnetic sublattices giving them a small but measurable net magnetisation, making them highly attractive for spintronic applications. Rare-earth–transition metal (RE:TM) alloy FiMs have a tuneable composition that controls the FiM magnetic compensation at which the net magnetisation vanishes, enabling perpendicular magnetic anisotropy (PMA) and enhanced spin–orbit torque (SOT) switching efficiency.

Recent experiments on RE:TM thin films with compositional gradients through the film thickness have demonstrated energy efficient, field-free SOT switching in such systems. These gradients have been suggested to induce transitions from in-plane (IP) to out-of-plane (OOP) or canted magnetisation and to promote a gradient-driven Dzyaloshinski-Moriya interaction (DMI) that creates chiral magnetic spin texture. These have been suggested as mediating the field-free SOT switching. However, to date there is no experimental evidence for these proposed mechanisms.

Here, XMaS/BM28 was used to experimentally profile the spatial distribution of the Gd magnetisation through the film thickness in compositionally graded GdCoFe films to map the regions of IP, OOP and canted magnetisation orientations in these novel material systems [1]. Two compositionally graded samples with positive and negative gradients were grown by co-sputtering with Gd ranges spanning 19 to 24 atomic %. A sketch of the positive gradient sample is shown in Fig. 6. These samples were specifically designed for X-ray resonant magnetic reflectivity (XRMR) at the Gd L_3-edge, with the materials and thicknesses of the underlayer, capping layer and magnetic layer optimised by simulations. The composition through the GdCoFe layer was obtained by secondary ion mass spectrometry (SIMS).

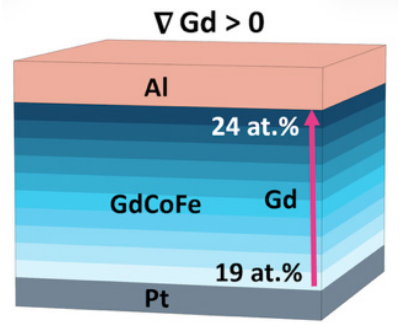

Fig. 6: Schematic of compositionally graded Gd:CoFe FiM thin-film sample.

The Gd magnetisation profile in the ∇Gd > 0 sample, derived from fitting of the XRMR data using GenX and the Gd SIMS data are shown together in Fig. 7. The results show a linear increase in Gd concentration but a non-linear in-plane Gd magnetisation, peaking at ~22 at.% Gd. Beyond this, the magnetisation drops to near zero, despite rising Gd content, giving a region with varying anisotropy and OOP magnetisation from 23-24 at.% Gd. The total Gd magnetisation is expected to be proportional to the local at.% of Gd, so comparing the expected total Gd magnetisation from SIMS, with the measured Gd magnetic scattering length density (SLD), the local angle of the Gd magnetisation was estimated (Fig. 8). This confirms the OOP regions and, unexpectedly, the magnetisation canting between 19~21 at.% Gd, possibly due to sperimagnetism. These magnetisation maps enable understanding and optimisation of field-free SOT switching.

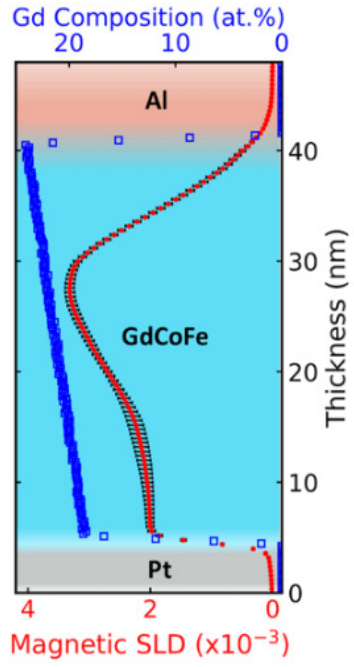

Fig. 7: In-plane Gd magnetic profile in 40 nm graded GdCoFe layer. Magnetic SLD (red dots) alongside Gd profile from SIMS.

[1] D. Rianto *et al.*, Commun. Mat. 6, 264 (2025).

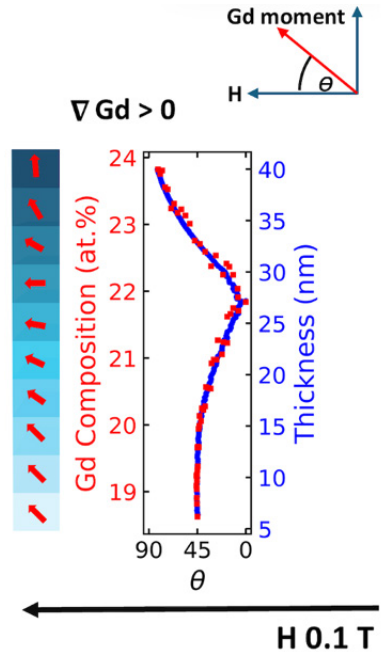

Fig. 8: Gd magnetisation angle as a function of depth and Gd at.% in the GdCoFe layer.

For more information, contact:

D. Atkinson,
Physics Department,
Durham University, UK.

del.atkinson@durham.ac.uk

Do capacitors work in polar region or deep space?

J. Vijayakumar, Y. Watier, P. Thompson, S. Guessasma, P. Tafforeau

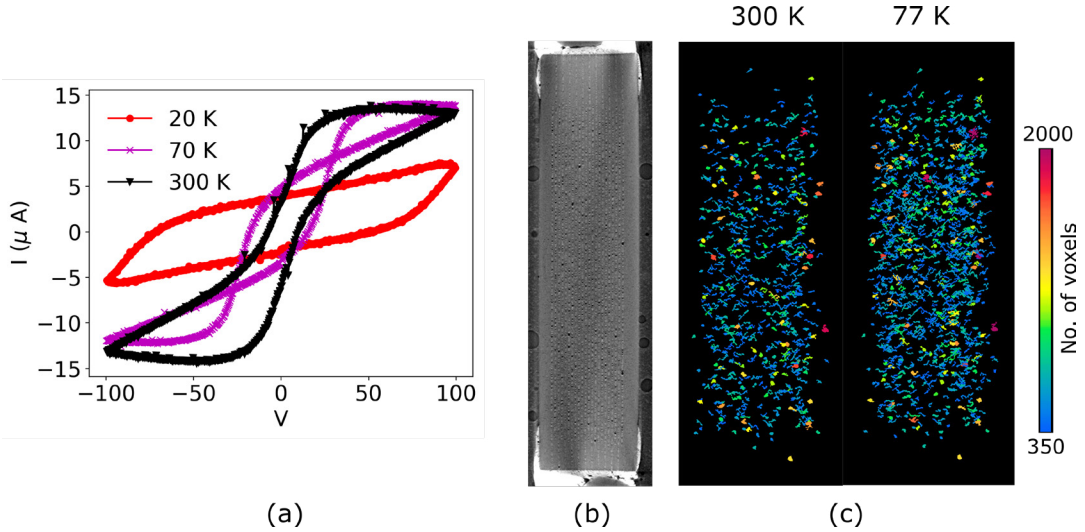

Fig. 9: (a) I-V curve of multilayer ceramic capacitor as a function of temperature. (b) Cross section of the multilayer capacitor showing multilayers and porosity. (c) 3D rendering of the pores across the capacitor volume at 300 K and 77 K. The colours represent individual volume as number of voxels (3D unit of pixel).

Electronic devices operate only within a fixed temperature window (e.g. 150 to -55°C). Outside a given temperature range, such as in polar region, such devices are usually encapsulated inside a temperature-controlled chamber. Electronic devices are composed of multiple electrical components; capacitors are one of the basic components sensitive to temperature. In commonly used capacitors, such as ceramic capacitors, the capacitance reduces with temperature. While this effect is well known, the microstructural changes inside such capacitors have never been investigated.

X-ray microtomography is a non-destructive imaging technique, where internal structures can be resolved in 3D. However, performing low temperature characterisation still remains a challenge. In this work, we have developed a cryo-microtomography setup at BM18 **[1]**, where samples can be imaged in a 77 K (-197°C) environment.

With the cryo-microtomography setup we obtained detailed information on the microstructural changes inside different commercial capacitors at 77 K between 3-5 µm resolution. Additionally, we conducted low temperature transport measurements using the offline facility of the XMaS/BM28 beamline to correlate the structural properties extracted from the BM18 X-ray images and the electrical properties from the I-V curves collected at BM28 down to 20 K **[2]**.

The electrical response of a multilayer ceramic capacitor (104 M5E) is shown in **Fig. 9a** as an example. The square loop I-V curve at 300 K becomes a 3-loop I-V curve at 70 K indicating the capacitance to vary with applied voltage, due to crack openings identified by the microtomography data (**Fig. 9b-c**). Our results suggest that the local strain induced by different materials in the capacitive layers can play a dominant role in the change of the capacitors electrical properties, potentially inducing changes in the permittivity or physical geometry of the capacitive structure.

We have demonstrated in this work that the combination of low temperature electrical characterisation and cryo-microtomography can be essential for the design of future capacitors/electronic devices to be operated in low temperature environment.

[1] J. Vijayakumar *et al.*, J. Synchrotron Rad. 37 (5), 16 (2024).
[2] J. Vijayakumar *et al.*, J. Eur. Ceram. Soc. 46 (4), 117966 (2026).

For more information, contact:

J. Vijayakumar,
ESRF, The European Synchrotron,
Grenoble, France.

jaianth.vijayakumar@esrf.fr

Dads, diet and bone development

A.J. Watkins, S. Sirovica, A.P. Morrell, O. Addison, R.A. Martin

Typically, our health in adulthood is seen as a product of our adult lifestyle such as poor diet, lack of exercise or smoking. However, there is a wealth of data connecting how we develop prior to birth and our risk for developing a range of diseases such as obesity, type 2 diabetes and heart disease. Similarly, studies have shown that our bone health is also shaped by the way we develop in the womb.

Typically, these studies have focused on maternal influences such as poor diet during pregnancy. However, we previously saw that offspring fetal bones, sired by male mice who had been fed a low protein diet (LPD) for several weeks prior to mating, displayed significant changes in their size and constituent hydroxyapatite lattice parameters **[1]**. Under the current study, we aimed to explore the mechanisms through which paternal LPD programmed offspring bone development and whether any changes persisted across generations.

We have shown previously **[2]** that fathers can shape the development of their offspring though both the sperm's genomic contribution and the fluid they are carried in (seminal plasma) at the time of mating. In the current study **[3]**, we generated offspring mice from males fed a LPD using their sperm, with or without the seminal plasma. Male first generation (F1) offspring were mated to create a second (F2) generation to assess the heritability of paternal bone effects.

We used micro-computed tomography (μ-CT) to study F1 and F2 offspring bone morphology focusing on the cortical and trabecular regions (highlighted in blue in **Fig. 10A**). Additionally, we used synchrotron X-ray diffraction (XRD) on XMaS/BM28 to obtain cortical bone hydroxyapatite crystallographic lattice parameters.

We observed that from just 3 weeks of age, neonatal F1 offspring derived from LPD fed males displayed differential femur cortical and trabecular bone morphology as assessed using μ-CT. Furthermore, we observed sperm and seminal plasma-specific influences on bone hydroxyapatite crystal lattice parameters. In adulthood (16 weeks of age), differences in femur bone morphology were still observed which associated with accompanying altered bone hydroxyapatite c-lattice parameters across the bone. Furthermore, in our second (F2) generation of offspring, differences in femur cortical and trabecular bone morphology were still evident (see **Fig. 10C**).

Interestingly, in sperm from our LPD fed fathers, we identified reduced expression of multiple extracellular matrix, transcription factor, growth factor and ossification genes.

Our study **[3]** shows that a father's diet at the time of conception can significantly shape the development and structure of his offspring's bones over multiple generations.

[1] A.J. Watkins *et al.*, Biochim Biophys. Acta Mol Basis Dis. 1863,1371 (2017).
[2] A.J. Watkins *et al.*, Proc. Natl. Acad. Sci. 115 (40),10064 (2017).
[3] S. Sirovica *et al.*, Function. 6(6), zqaf051 (2025).

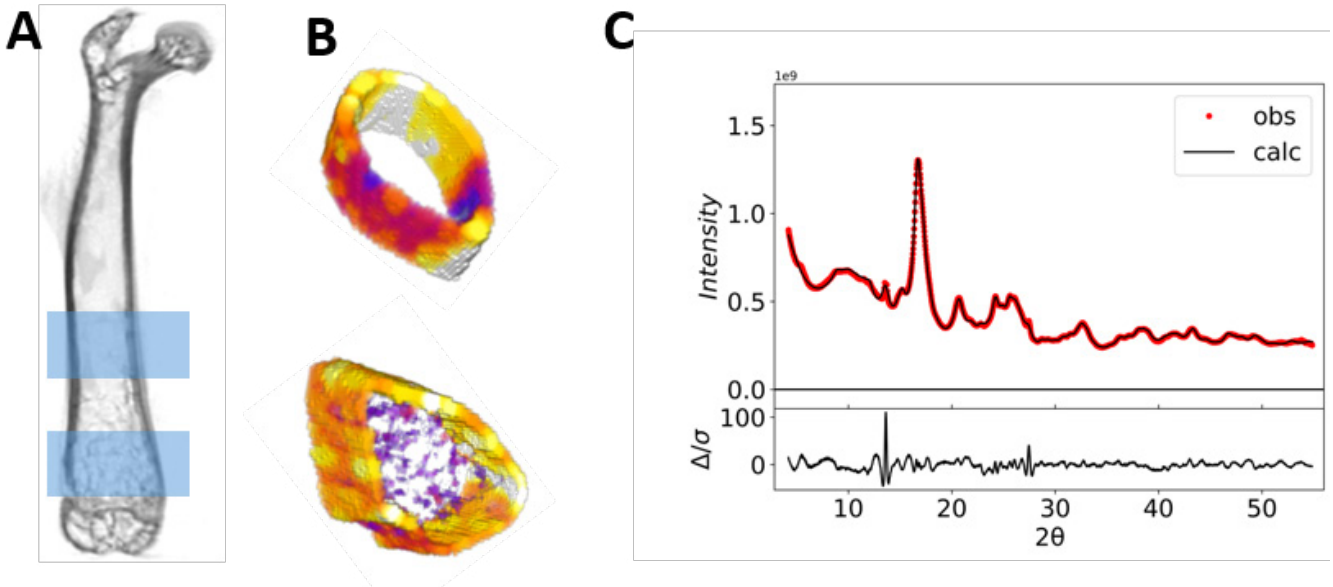

Fig. 10: (A) Representative μ-CT image of an offspring femur highlighting (blue boxes). (B) cortical and trabecular regions. (C) Intensity (azimuthal integration) of the XRD pattern across the femur cortical bone.

For more information, contact:

A. J. Watkins
School of Medicine and Population Health, University of Sheffield, UK.

a.watkins@sheffield.ac.uk

Investigating the site of the rare-earth elements in clays

M.P. Smith, A.A. Finch, A.M. Borst

The rare-earth elements (REE – the lanthanides, plus yttrium and scandium) are critical elements for their role in renewable energy generation and low carbon transport. They have two main geological sources – carbonatite (igneous carbonate rocks) and ion adsorption deposits (IADs), the latter of which are the main global source of the heavy REE. IADs are REE-rich soils and weathered rock derived from the breakdown of granite (**Fig. 11A**), from which the REE can be easily leached using low strength reagents. For the last decade we have been working on the structural site of the REE in clays from these deposits. This is important both to understand the formation of deposits (and so help predict where they might be found) and to guide development of lower impact and higher recovery leaching methods.

Previously we used yttrium (as a proxy for the REE) K-edge X-ray absorption spectroscopy (XAS) to determine that the REE were held as 8 or 9 co-ordinated aqueous complexes held by electrostatic forces on the surface of kaolinite clay [1]. However, it is difficult to extend this study to the other REE because natural materials host all the lanthanides and their X-ray absorption lines overlap at L-edge energies. This means we cannot directly investigate the change in co-ordination and bonding across the lanthanide series as we did for Y.

New developments at the XMaS/BM28 beamline mean that higher energies are now achievable, with the monochromator allowing use of X-rays up to ~47 keV. We can thus measure XAS at the K-edge of the light lanthanides at 39-47 keV. In October 2025 we measured the extended X-ray absorption fine structure (EXAFS) across the K-edge of cerium, neodymium and samarium in REE bearing clay samples from China, Madagascar and Finland (**Fig. 11B**). The spectra were collected in fluorescence using the 7-element Mirion HPGe detector. The data allow us to determine the oxidation state of Ce, and we show that it is present as CeO_2 in some samples – geochemically separating it from other trivalent REE. However the data indicate Ce(III) in other samples (**Fig. 11C**). The coordination of Nd in the clays is still being analysed, but whilst Ce(IV) is surrounded by a second shell in a crystal lattice, this is less clear in Nd, and consistent with a surface adsorbed structure.

In future experiments, we will measure La absorption to obtain high quality data to high k-range to determine if La is adsorbed or incorporated into a crystal lattice. This will allow us to fully extrapolate the co-ordination and bonding of clay surface adsorbed REE.

[1] A. Borst *et al.*, Nat. Commun. 11, 4386 (2020).

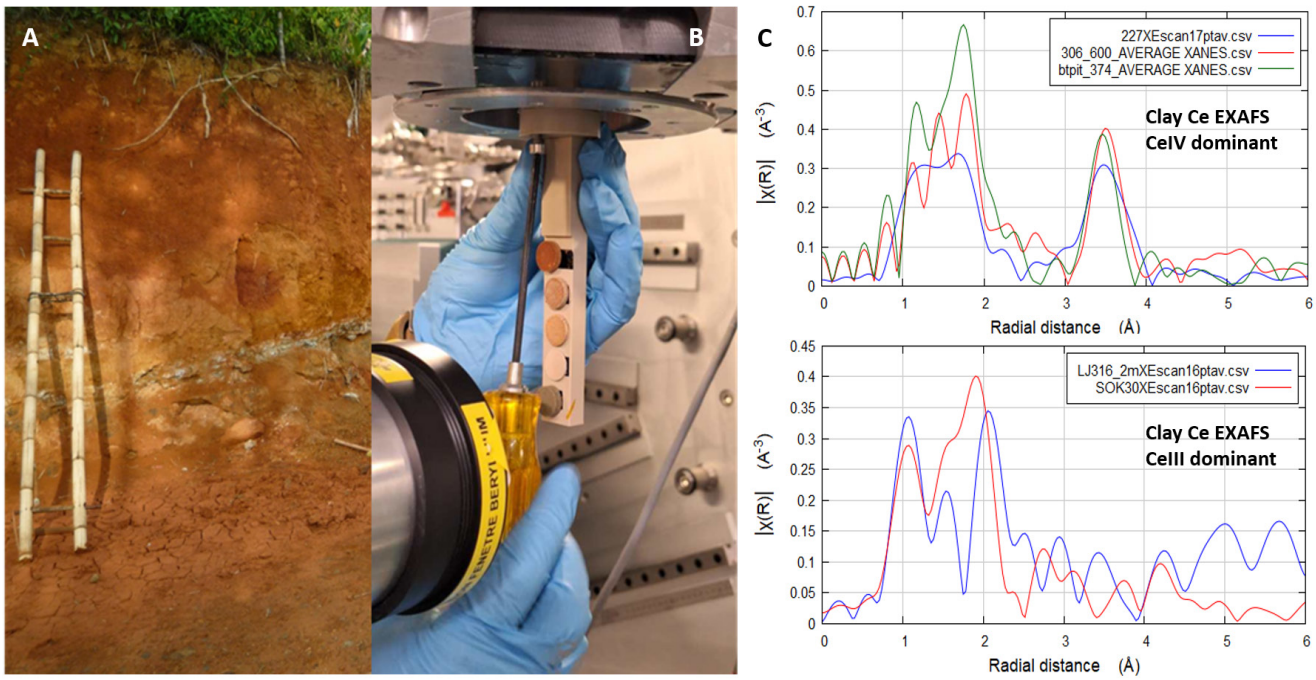

Fig. 11: Rare-earth mineralised soils from the macro- to the nano-scale. (A) An ion adsorption clay deposit in laterite from Madagascar. (B) Loading pressed pellets of laterite clays at the XMaS/BM28 beamline. (C) Fourier transformed Cerium K-edge EXAFS from lanthanide bearing clays.

For more information, contact:

M. Smith,
School of Applied Sciences,
University of Brighton, UK.

martin.smith@brighton.ac.uk

Triclinic liquid crystal of counter-rotating squashed double helices

Y.N. Xue, Y.X. Li, Y.M. Tang, S.G. Yang, R.Y. Ji, L. Cseh, F. Liu, X.B. Zeng, G. Ungar

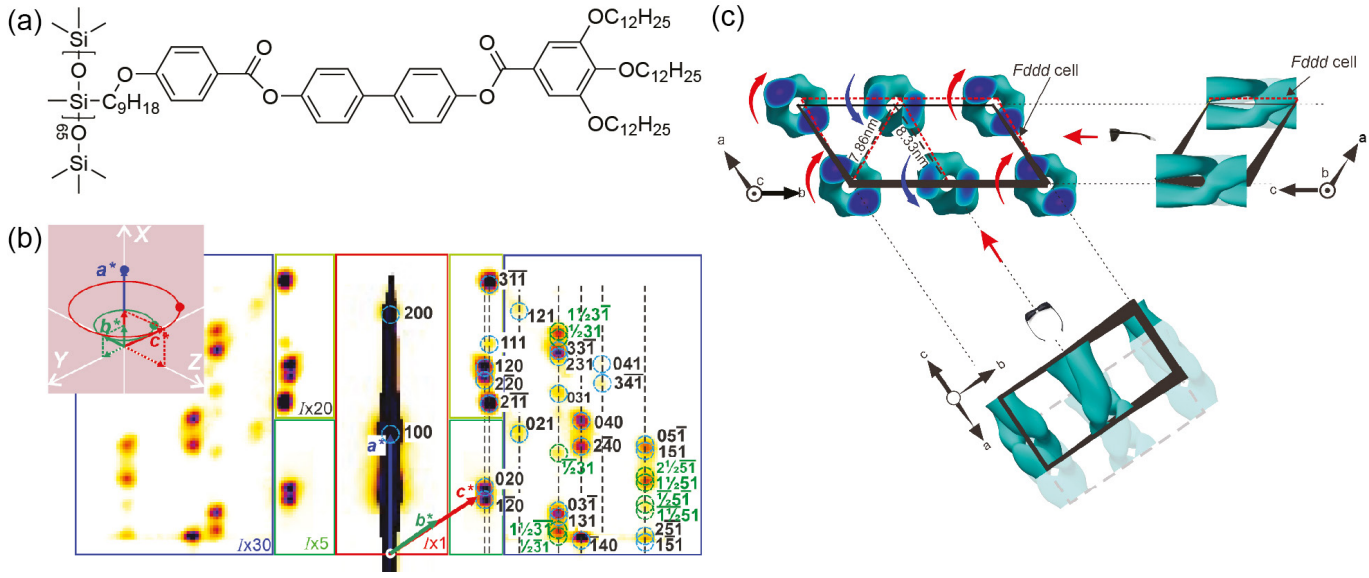

Fig. 12: (a) Chemical structure of the side-chain LC polymer. (b) GI-SAXS pattern revealing the triclinic lattice. (c) Reconstructed electron density maps of the triclinic phase viewed along different directions.

Helical and especially double-helical structures have intrigued scientists and the general public ever since the discovery of the DNA double helix. Helix is a topological solution of a system's conflicting tendencies to order. For example, most polymers crystallise in a helical conformation, keeping the chains straight overall so they can pack sideways efficiently, while avoiding side-group clashes by their twisting around the helical axis.

When the constituent molecules are chiral, the chirality of the helix they form is determined by their chiral interactions. In liquid crystals however, columns self-assembled from achiral molecules do not normally possess long-range chiral order. This is because a 1D column cannot have long-range order according to the laws of thermodynamics, and helices will not form unless the columns act cooperatively and without crystallisation (to keep the liquid crystalline LC phase).

In a recent study of a side-chain polymer [1], where mesogenic side-groups are attached to a central polysiloxane chain (Fig. 12a), we have observed the formation of 3D ordered liquid crystalline columnar phases where each column is a double helix. The aromatic cores of the side-groups form the two strands of the double helix, winding around the central polysiloxane chains.

A metastable columnar phase with higher symmetry is observed on cooling of the polymer from melt. It has an orthorhombic face centred unit cell and consists of eight double helical columns, four of them left- and four right-handed. Intriguingly, this metastable phase transforms to another with much lower triclinic symmetry. Grazing incidence small angle X-ray scattering (GI-SAXS) experiment on oriented thin films (Fig. 12b), carried out at XMaS/BM28 allowed the unequivocal indexing of the diffraction pattern.

The formation of a triclinic LC phase is unusual in that the stablisation of LC phases is typically entropical. Consequently phases with higher symmetries are normally preferred. Our studies reveal that the twisting of the double helix around the helical axis is far from uniform: they contain alternating nearly straight "splay" segments interrupted by sharply twisted "splay recovery" segments (Fig. 12c). Such non-uniform twisting is believed to be the reasons behind the distortions to the original high symmetry lattice, due to the more anisotropic nature of inter-columnar interactions.

So far LC polymers have mostly mirrored the phases of low-molecular LCs, but this report shows that polymers offer new modes of self-assembly of their own. It calls for re-evaluation of some established models of complex self-assembly.

[1] Y.N. Xue *et al.*, J. Am. Chem. Soc. 147, 19711 (2025).

For more information, contact:

X.B. Zeng,
School of Chemical,
Materials and Biological Engineering,
University of Sheffield, UK.

x.zeng@sheffield.ac.uk

Interconnected donor-acceptor-additive structural effects on organic solar cells

E. Gutiérrez-Fernández, A. Harillo-Baños, E. Solano, O. Bikondoa, J. Gutiérrez, A. Tercjak, M. Campoy-Quiles, S. Riera-Galindo, J. Martín

On the way to manufacture flexible, light and performant solar cells, many researchers have focused on novel semi-rigid semiconducting polymers and small molecules. These two materials can be physically mixed into a photoactive layer and hence into a solar cell. Future commercialisation of these devices will be possible as long as we understand how the components influence each other in the photoactive layer to form a stable micro- and nano-structure [1].

We studied the structure of a single-junction PM6:Y6 solar cell mixed with the solvent additive 1-chrolonaphtelene (1-CN). Despite the amount of publications on this system, it was not clear how the three components affect each other to modify the entangled structure and guide the photovoltaic efficiency [2]. In this work [3], we demonstrate that one key to improve the power conversion efficiency (PCE) of the device is to keep a well-blended phase of PM6 and Y6. The presence of non-mixed polymeric (PM6) aggregates is correlated with a low efficiency (Fig. 13a). Y6 and the solvent additive trigger a dilution effect on PM6 (Fig. 13c-d) and hence its mixing with Y6, improving the performance even in PM6-rich devices (Fig. 13b). A good balance between donor and acceptor is key to increase the efficiency by just improving the network percolation. Here, we prove that the solvent additive has an equivalent effect on PM6-rich cells.

At the NCD beamline (ALBA synchrotron, Barcelona), we identified the effect of the solvent additive and the splitting of the Bragg peak associated with the π-π stacking of conjugated molecules, that takes place when Y6 diffuses out of the PM6:Y6 matrix and crystallises (Fig. 14a). At XMaS/BM28 (ESRF, Grenoble), we proved that Y6 is able to diffuse out of the matrix only if its content is higher than PM6 and aided by the presence of the solvent additive (Fig. 14b-c).

We conclude that in PM6:Y6 and likely in similar systems, a good efficiency value can be achieved if the polymer is fully mixed in a single phase with the acceptor molecule. This effect can be tuned by increasing the acceptor content or by adding a solvent additive. By combining both components, the acceptor is able to diffuse and crystallise. Such moderate crystallisation thus improves electronic paths but may potentially degrade the structural stability of the system.

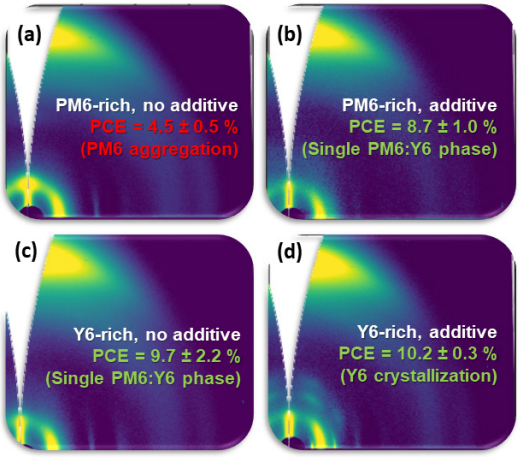

Fig. 13: Grazing incidence wide angle X-ray scattering (GIWAXS) patterns of PM6:Y6 cells in the three different regimes.

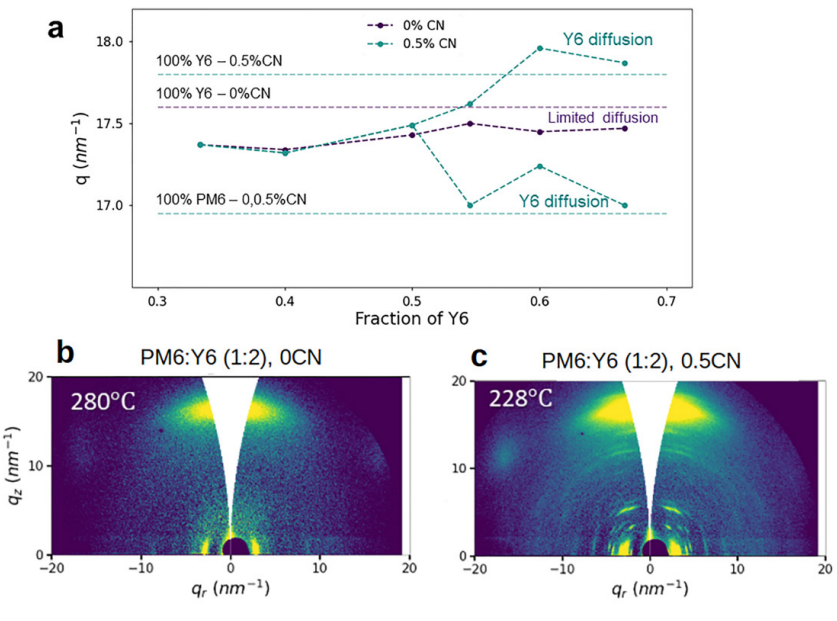

Fig. 14: (a) q-position of π-π stacking Bragg peak for all the studied systems. (b-c) GIWAXS patterns of Y6-rich cells, without (b) and with (c) solvent additive above the Y6 crystallisation temperature.

[1] S. Shoaee *et al.*, Adv. Mater, 36, 20 (2024).
[2] S. Marina *et al.*, Mater. Horiz. 9, 4, (2022).
[3] E. Gutiérrez-Fernández *et al.*, J. Mater. Chem. C. 13, 22722 (2025).

For more information, contact:
E. Gutiérrez-Fernández,
ESRF, The European Synchrotron,
Grenoble, France.
edgar.gutierrez-fernandez@esrf.fr

A new electrode for rechargeable zinc-ion batteries

Z. Li, A.W. Robertson

Rechargeable batteries are critical for a sustainable energy future, but current technologies rely on scarce resources and are often expensive. Aqueous zinc-ion batteries (ZIBs) are attractive because zinc is abundant, safe and recyclable, and its water-based electrolytes are environmentally friendly. However, finding a cathode for these batteries that can reversibly cycle the zinc ion without damage and with reasonable efficiency is challenging. We have developed a new cathode material suitable for use in a zinc-ion battery, and used XMaS/BM28 to better understand how the zinc ions are stored and released in this new system [1].

To understand how the new cathode material, a cation-disordered rocksalt $ZnMnO_2$, behaves during battery operation, we used X-ray absorption spectroscopy (XAS), specifically the X-ray absorption near edge structure (XANES) region. The spectra were collected in transmission mode (**Fig. 15**). In this study, XANES was applied to monitor the manganese oxidation state of the cathode during cycling. The experiments showed that energy storage with this cathode involves Mn dissolution and redeposition, alongside a structural transformation to a spinel phase that enables reversible Zn^{2+} intercalation.

The XANES was critical for revealing the change in Mn oxidation state, which in turn confirmed this cycling mechanism (**Fig. 16**). XANES of the Mn K-edge was used to estimate the valence by comparison with reference samples (dashed lines). By taking measurements from pristine (P rest), fully charged (FC) and fully discharged (FD) cathode samples, we tracked the change in oxidation state across different parts of the battery recharge/discharge cycle.

These results, taken in coordination with other techniques such as mass spectrometry and X-ray diffraction, showed that as the Mn valence exhibits only a slight decrease during discharge, the battery capacity must instead originate from another mechanism. We were able to show that this is due to the reversible dissolution and redeposition of the Mn into and out of the aqueous electrolyte.

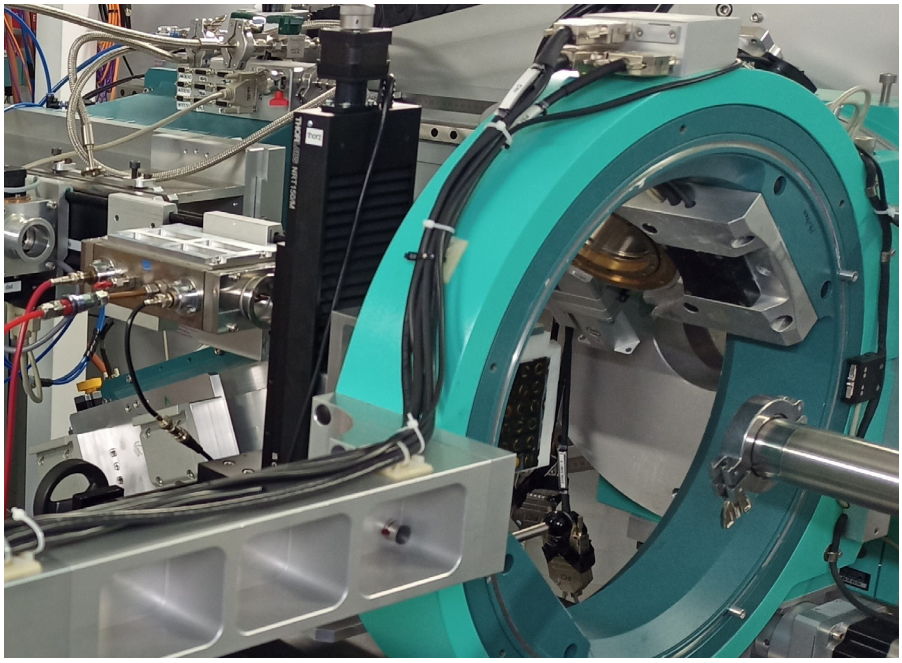

Fig. 15: Experimental setup used at XMaS. The ex-situ samples were pre-mounted on a rack. The transmission XANES spectra were measured using two ionisation chambers.

We are now working to understand the relationship between the evolving morphology of the redeposited MnO_2 and the cathode's performance and degradation.

[1] Z. Li *et al.*, Energy Environ. Sci. 18, 10135 (2025).

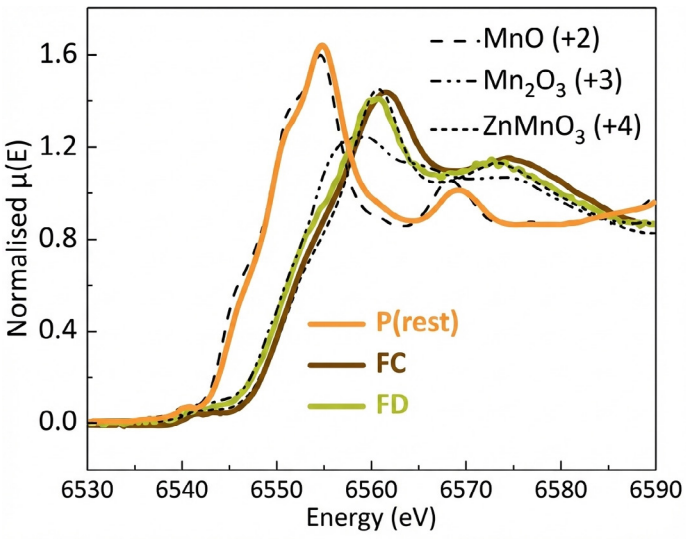

Fig. 16: Mn K-edge XANES spectra of the cathode collected at different states of charge, along with reference spectra (dashed lines) of different oxidation states of Mn.

For more information, contact:

A. Robertson,
Department of Physics,
University of Warwick, UK.

alex.w.robertson@warwick.ac.uk

A new window into catalysts: operando anomalous diffraction and X-ray absorption at the XMaS beamline

D. Wardecki, P. Thomson, K. Mlekodaj, M. Dowsett, M. Adriaens, A. Knorpp, C. Dejoie, K. Góra-Marek, J. van Bokhoven, M. Newton, P. Rzepka

Understanding how atomic positions and catalytically active sites evolve during a chemical reaction is essential for explaining and improving the behaviour of functional materials. A new *operando* setup on the XMaS/BM28 beamline, described by our group [1], allows the combination of **anomalous powder X-ray diffraction (APXRD) with X-ray absorption spectroscopy (XAS)** in a single experiment. A scanning flat-panel detector (Pilatus3 300K) records diffraction images across a wide angular range, while interleaved XAS spectra track the chemical state of selected elements. This integrated approach provides simultaneous element-specific insight into both structure and electronic state under true working conditions.

APXRD is particularly powerful because tuning the X-ray energy close to an absorption edge selectively enhances the scattering of one chosen element, such as copper, without altering the rest of the lattice. This highlights the sparse amounts of catalytically active species and pinpoints their positions within a complex framework. The XMaS setup extends this capability to *operando* environments, capturing high-quality diffraction patterns even at low photon energies, where static detectors would normally restrict the accessible scattering Q-range.

The potential of this method becomes clear when applied to Cu-exchanged mazzite (Cu-MAZ), a zeolite known for efficiently converting methane to methanol via an oxygen-looping process. Earlier studies [2,3] had shown that the active sites in Cu-MAZ consist of two closely spaced Cu–OH monomers located at neighbouring entrances of the 8-membered rings [2]. However, how these copper species behave during activation, reaction, hydration and migration could not be fully resolved without *operando* structural information [3].

With the new XMaS setup, the positions and oxidation states of copper can be tracked simultaneously as the catalyst cycles through oxygen activation and methane reaction. The diffraction data reveal how copper redistributes between distinct crystallographic sites, while XAS confirms the associated Cu(II)/Cu(I) redox behaviour. Together, these measurements give a clear picture of how active Cu-monomer pairs form, persist or reorganise under different conditions, providing direct evidence of the structural dynamics that control catalytic performance.

This combined APXRD-XAS methodology marks a significant step forward in *operando* characterisation. By uniting crystallographic and spectroscopic information in real time, it allows researchers to observe catalytically important copper species as they respond to reaction conditions inside the zeolite framework. Applied to Cu-MAZ, it reveals the subtle structural rearrangements that underpin one of the most promising routes for direct methane-to-methanol conversion and opens new possibilities for designing more active and robust catalytic materials. Although demonstrated here on Cu-zeolites, the approach is broadly applicable and can be used in any system where real-time monitoring is needed. APXRD selectively enhances the scattering of an element whose speciation is tracked simultaneously by spectroscopy.

[1] D. Wardecki *et al.*, J. Appl. Cryst. 58, 1778 (2025).
[2] A. Knorpp *et al.*, Angew. Chem. Int. Ed. 60, 5854 (2021).
[3] J. Wieser *et al.*, Angew. Chem. Int. Ed. 63, e202407395 (2024).

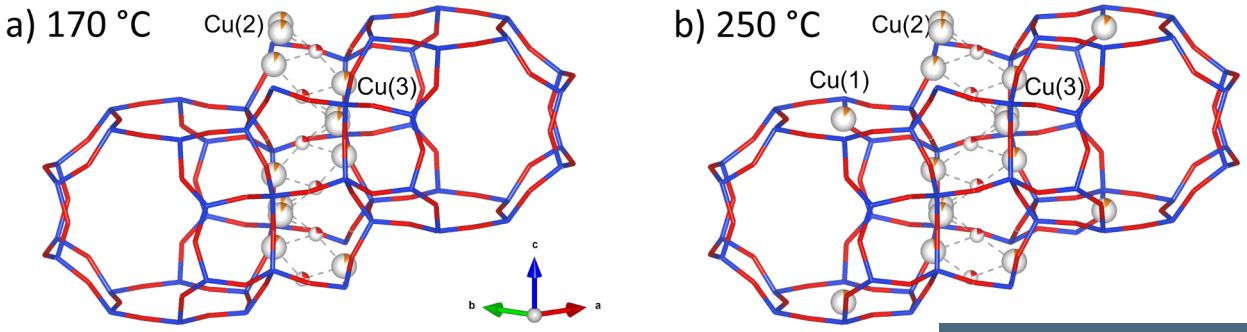

Fig. 17: Representations of the copper positions within the Cu-MAZ structure as a function of temperature during aerobic activation.

For more information, contact:

P. Rzepka, Department of Structure and Dynamics in Catalysis,

J. Heyrovský Institute of Physical Chemistry, Czech Academy of Sciences, Czechia.

przemyslaw.rzepka@jh-inst.cas.cz

Investigating metal-support interactions in ceria zirconia catalysts

L. Costley-Wood, N. Flores-Gonzales, D. Decarolis, D. Thompsett, T. Hyde, E. Gibson

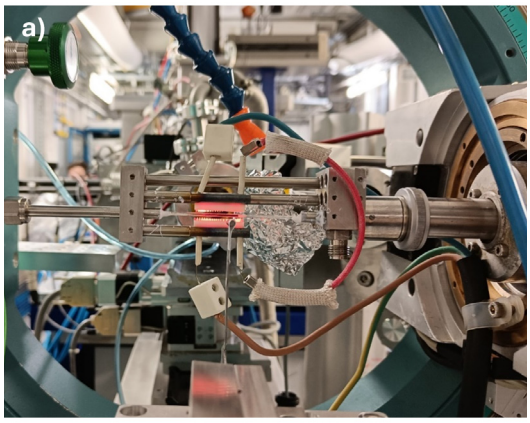

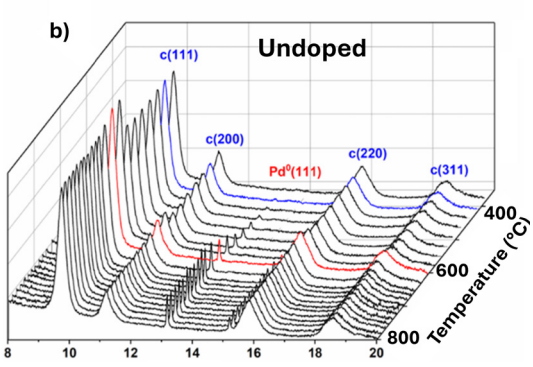

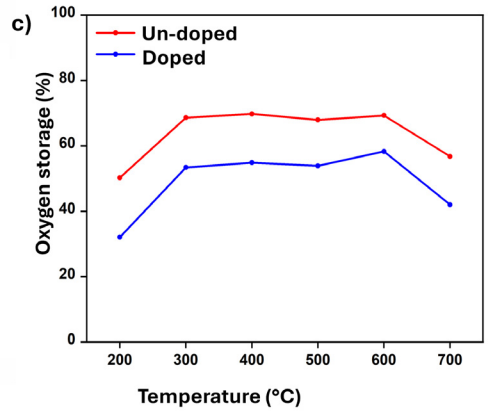

Fig. 18: (a) Photo of the high temperature cell on XMaS/BM28.
(b) PXRD during cooling of undoped $Pd/CeZrO_2$.
(c) Oxygen storage capacity of doped and undoped $Pd/CeZrO_2$.

Ceria zirconia is an essential component of catalytic converters, the emission-reduction technology used in petrol cars. Despite the rise of electric vehicles, in 2024 around 52% of all new vehicle registrations were for non-hybrid petrol cars. Ceria zirconia is valued for its ability to store and release oxygen, which helps to regulate the oxygen-to-fuel ratio in the exhaust. This enables the active catalytic metal, palladium (Pd), to function effectively over a wide range of operating conditions [1].

The strength of the interaction between Pd and the ceria zirconia surface, where Pd nanoparticles are anchored, can influence both catalyst performance and lifetime [2]. To investigate this, we compared two different ceria zirconia materials: one undoped and one doped with rare-earth elements. These dopants improve the stability of the support at high temperature and assist in the removal and replenishment of oxygen under oxygen-rich or oxygen-poor conditions [3].

We performed a combined high-temperature powder X-ray diffraction (PXRD) and X-ray absorption near-edge spectroscopy (XANES) experiment under air. A custom reaction cell, based on a previously published design, was constructed for this purpose (Fig. 18a) [4]. The aim was to observe the transition between palladium oxide and metallic palladium and to infer the strength of the metal-support interaction. When this interaction is weaker, Pd nanoparticles become more mobile. During the oxide-to-metal transition, this can cause the particles to re-disperse into very small sizes, making them effectively invisible to XRD. Measuring both PXRD and XANES therefore allowed us to track the chemical state even when the particles were too small to diffract.

The results showed that, on the doped support, the re-dispersion of palladium oxide is more efficient, and more of the metal is able to re-form the oxide phase (Fig. 18b). XANES confirmed that metallic Pd was present even at temperatures where no Pd reflections were visible in XRD.

By combining these measurements with other complementary synchrotron experiments and with catalyst performance testing at Johnson Matthey, we demonstrated that rare-earth doping weakens the metal-support interaction, which negatively affects catalytic activity (Fig. 18c). The Pd becomes less able to benefit from the oxygen storage of the ceria zirconia. However, the improved thermal stability afforded by the dopants is essential for maintaining catalyst performance over lifetimes exceeding 10 years. These insights will support the development of improved catalyst materials in future applications [5].

[1] S. Rood *et al.*, J. Automob. Eng. 234, 936 (2020).
[2] C. Qiu *et al.*, ACS Catal. 12, 9125 (2022).
[3] A. Papavasiliou *et al.*, Appl. Catal. A 382, 73 (2010).
[4] P. Chupas *et al.*, J Appl. Cryst. 41, 822 (2008).
[5] L. Costley-Wood *et al.*, Chem. Mater. 37, 7214 (2025).

For more information, contact:
L. Costley-Wood,
Department of Chemistry,
UCL, UK.
l.costley-wood@ucl.ac.uk

ACCESS TO SYNCHROTRON AND OFFLINE FACILITIES

Two proposal review rounds are held each year. Deadlines for applications to make use of the National Research Facility (CRG) time are normally 1st April and 1st October for the scheduling periods August to February and March to July, respectively.

Applications for beamtime must be submitted electronically via the ESRF web page: **www.esrf.eu**. Select **"Users & Science"**, then choose **"Applying for beamtime"** from the drop-down list. On the right hand side, you can consult the instructions to submit your proposal and access the **"User Portal"**. Enter your surname and password and select **"Proposals/Experiments"**. Follow the instructions carefully — you must choose **"Collaborative Research Group"** and **"BM28 (XMaS) UK Materials Science CRG Beamline"** at the appropriate stage in the process. If you experience any problems, please contact Laurence Bouchenoire (**bouchenoire@esrf.fr**). Technical specifications and instrumentation available are described on the XMaS web page (**www.xmas.ac.uk**). All sections of the form must be filled in. Particular attention should be given to the safety aspects with the name and characteristics of your samples completed carefully. Experiments requiring special safety precautions such as the use of electric fields, lasers, high pressure cells, dangerous substances, toxic substances and radioactive materials, must be stated clearly in the proposal. Moreover, any ancillary equipment supplied by the user must conform to the appropriate French regulations. Further information may be obtained from Martine Moroni, the ESRF Experimental Safety Officer for CRG beamlines (**martine.moroni@esrf.fr**, tel: +33 4 76 88 23 69). Please indicate your date preferences, including any dates that you would be unable to attend if invited for an experiment. This will help us to produce a schedule that is satisfactory for all.

When preparing your application, please consider that access to the National Research Facility is reserved for UK based researchers. Collaborations with EU and international colleagues are encouraged, but the proposal must be led by a UK based principal investigator. It must be made clear how any collaborative research supports the wider UK science base. Applications without a robust link to the UK will be rejected and should instead be submitted directly to the ESRF using their public access route.

Access to the XMaS beamline is also available for one third of its operational time to the ESRF's user community. Applications for beamtime within that quota should be made in the **ESRF's proposal rounds (application deadlines early March and September**). Applications for the same experiment may be made to both XMaS directly and to the ESRF. Obviously, proposals successfully awarded beamtime by the ESRF will not then be given additional time in the XMaS allocation.

An experimental report on completed experiments must be submitted electronically, following the ESRF model. The procedure for submitting experimental reports follows that for the submission of proposals. Please follow the instructions on the ESRF's web pages carefully. **Reports must be submitted within 3 months of the experiment**. Note that the abstract of a publication can also serve as the experimental report! Please also remember to fill in the XMaS end of run survey form on completion of your experiment, which is available on the website (**https://bit.ly/3JM6E7q**).

Assessment of Applications

The independent Peer Review Panel considers the proposals, grades them according to scientific excellence, adjusts the requested beam time if required, and recommends proposals to be allocated beam time on the beamline. Experimental reports will also form part of the assessment criterion. Proposals which are allocated beamtime must meet ESRF safety and XMaS technical feasibility requirements. Following each meeting of the Peer Review Panel, proposers will be informed of the decisions taken and feedback provided.

APPLICATIONS FOR OFFLINE FACILITY TIME

Submit your application directly on the XMaS web site: **www.xmas.ac.uk**. Select **"XMaS Offline Facilities"** and then **"Application for Offline Facilities"**. Follow the instructions carefully and do not forget to upload your 1-2 page proposal at the end of the application form. Please contact the local staff to discuss any potential experiments. Successful offline proposals will be run as in-house experiments. We will complete the safety form with the information supplied in your application form as well as arrange site passes and any accommodation that may be required. As for synchrotron beamtime, offline users normally stay in the ESRF guest house or off-site hotels.

The XMaS facility implements transparent policies and procedures to guarantee that access is based on scientific excellence only. In partnership with the ESRF Safety office, we will endeavor to ensure that the facility can accommodate any user, but this may require an individual needs assessment. If you have any questions about accessing the facility at any stage of the application or experimental processes, please do not hesitate to get in touch.

Living allowances

These are €90 per day per beamline user — the equivalent actually reimbursed in sterling (see **www.xmas.ac.uk/user_information/ for details**). XMaS will support up to 3 users per synchrotron experiment and only 1 on the offline laboratories. For experiments which are user intensive, additional support may be available. The ESRF hostel still appears adequate to accommodate all our users, though CRG users will always have a lower priority than the ESRF's own users. Do remember to complete the "A-form" when requested to by the ESRF, as this is used for hostel bookings, site passes and to inform the safety group of attendees.

Beamline people

ONSITE TEAM

Didier Wermeille
didier.wermeille@esrf.fr
is the Beamline Responsible who, in partnership with the Directors, oversees the activities of the user communities as well as the programmes and developments that are performed on the beamline. He is also the beamline Safety Representative. His expertise spans crystallography, high resolution diffraction, surface studies, magnetic scattering and electric field measurements.

Laurence Bouchenoire
bouchenoire@esrf.fr
is the Beamline Coordinator. She looks after beamline operations and can provide you with information about the beamline, application procedures, scheduling, etc. Laurence should normally be your first point of contact. Her expertise is in magnetic scattering including polarisation dependence.

Oier Bikondoa
oier.bikondoa@esrf.fr
is Beamline Scientist with expertise in soft matter materials, (GI)-SAXS/WAXS, surface and reflectivity studies.

Paul Thompson
pthompso@esrf.fr
is the contact for instrument development, technical support, sample environments including electric field, liquid cells and catalysis.

Rachel Kilbride
rachel.kilbride@esrf.fr
is a PDRA specialised in organic semiconductors.

Florence Legg
florence.legg@esrf.fr
is a PDRA working on actinide systems for the nuclear fuel research.

PROJECT DIRECTORS

Chris Lucas **clucas@liv.ac.uk**

Tom Hase **t.p.a.hase@warwick.ac.uk**

and Yvonne Grunder
yvonne.grunder@liverpool.ac.uk
continue to travel between the UK and France to oversee the operation of the beamline.

Malcolm Cooper
m.j.cooper@warwick.ac.uk
remains involved in the beamline operation as an Emeritus Professor at the University of Warwick.

PROJECT ADMINISTRATORS

Katherine Norman
katherine.norman@warwick.ac.uk

and Julie Clark
Julie.Clark@liverpool.ac.uk
are the administrators on the project, based in the Department of Physics at Warwick and Liverpool, respectively. Katherine is the point of contact for user T&S claims and co-ordinates the annual XMaS Scientist Experience.

THE PROJECT MANAGEMENT COMMITTEE

The current membership of the committee is as follows:
C. Nicklin (chair), DLS.
L. Behrooz, EPSRC.
M. Alfredsson, Uni. of Kent.
M. Cain, Electrosciences Ltd.
A. Beale, Uni. College London.
K. Edler, Uni. of Lund.
P. Quinn, STFC.
S. Langridge, ISIS.
R. Weatherup, Uni. of Oxford

In addition to the above, the directors, the chair of the Peer Review Panel, the CRG Liaison T. Buslaps and the beamline team are in attendance at the meetings which happen twice a year.

THE PEER REVIEW PANEL

The current membership of the panel is as follows:
R. Arrigo (chair), Uni. of Salford.
A. Hector, Uni. of Southampton.
E. Heeley, Open University.
M. Skoda, ISIS.
K. Syres, Uni. of Central Lancashire.
L. Ishibe-Veiga, DLS.
M. Senn, Uni. of Warwick.

In addition, either Chris Lucas, Yvonne Grunder or Tom Hase attends their meetings in an advisory role.

PUBLISH PLEASE!!... and keep us informed

One of the important XMaS KPIs is the number and quality of publications. We ask you to provide us (**xmas@esrf.fr**) with the reference and DOI whenever a new paper is published. Alternatively, you can submit your new publication reference directly through a form on our web site (**https://bit.ly/2Gja4zX**). Please also let us know about other impact generated as a result of XMaS work.

IMPORTANT!
It is important that we acknowledge the support from EPSRC in any publications. When beamline staff have made a significant contribution to your scientific investigation you may naturally want to include them as authors. Otherwise we ask that you add an acknowledgement of the form:

"XMaS is a UK national research facility supported by EPSRC. We are grateful to all the beamline staff for their support."

Editor: Laurence Bouchenoire - Graphic Designer: Sylvie Quercia - February 2026

XMaS the UK-CRG

XMaS (BM28)
the UK Materials Science Beamline

ESRF - The European Synchrotron
71 avenue des Martyrs, CS 40220
38043 Grenoble Cedex 9,
France

Tel: +33 (0)4.76.88.25.80
xmas@esrf.fr

@xmasbm28.bsky.social

@XMaS: The UK Materials Science Facility at the ESRF

www.xmas.ac.uk

UNIVERSITY OF LIVERPOOL
UKRI Engineering and Physical Sciences Research Council
WARWICK THE UNIVERSITY OF WARWICK